ESCRT ubiquitin-binding domains function cooperatively during MVB cargo sorting

S. Brookhart Shields,[1] Andrea J. Oestreich,[2] Stanley Winistorfer,[1] Doris Nguyen,[2] Johanna A. Payne,[2] David J. Katzmann,[2] and Robert Piper[1]

[1]Department of Molecular Physiology and Biophysics, University of Iowa, Iowa City, IA 52240
[2]Department of Biochemistry and Molecular Biology, Mayo Clinic College of Medicine, Rochester, MN 55905

Ubiquitin (Ub) sorting receptors facilitate the targeting of ubiquitinated membrane proteins into multivesicular bodies (MVBs). Ub-binding domains (UBDs) have been described in several endosomal sorting complexes required for transport (ESCRT). Using available structural information, we have investigated the role of the multiple UBDs within ESCRTs during MVB cargo selection. We found a novel UBD within ESCRT-I and show that it contributes to MVB sorting in concert with the known UBDs within the ESCRT complexes. These experiments reveal an unexpected level of coordination among the ESCRT UBDs, suggesting that they collectively recognize a diverse set of cargo rather than act sequentially at discrete steps.

Introduction

Many integral membrane proteins targeted for lysosomal degradation are ubiquitinated and sorted into vesicles that bud from the limiting membrane into the lumen of endosomes during the biogenesis of multivesicular bodies (MVBs; Piper and Katzmann, 2007). Cargo selection during MVB sorting is dependent on several endosomal protein complexes known as endosomal sorting complexes required for transport (ESCRT). Several ESCRT components contain ubiquitin (Ub)-binding domains (UBDs) that may act as receptors for ubiquitinated membrane proteins. For instance, ESCRT-0, comprised of yeast Vps27 and Hse1 or mammalian Hrs and STAM (signal transducing adaptor molecule), contains Ub-interacting motifs (UIMs) required for MVB sorting of ubiquitinated cargo (Bilodeau et al., 2002; Shih et al., 2002; Piper and Katzmann, 2007). The Ub E2 variant (UEV) domain in Vps23/TSG101, an ESCRT-I component in yeast/mammalian cells, and the GLUE (GRAM-like Ub binding in EAP45) or Npl4 zinc finger (NZF) domains of Vps36, an ESCRT-II component, also contain UBDs that have been implicated in MVB cargo selection (Katzmann et al., 2001; Alam et al., 2004; Slagsvold et al., 2005). This had led to a model in which Ub cargo is passed sequentially from ESCRT-0 to ESCRT-I and to ESCRT-II for final deposit into the forming lumenal vesicles (Katzmann et al., 2002; Gruenberg and Stenmark, 2004; Hurley, 2008). Previous studies have indicated the importance of these UBDs during MVB sorting; however, recent high resolution structures that detail Ub interactions have enabled a more precise approach to dissect the contributions of these UBDs to MVB sorting (Alam et al., 2004, 2006; Sundquist et al., 2004; Teo et al., 2004; Hirano et al., 2006). Surprisingly, we found that mutant forms of Vps23 and Vps36 unable to bind Ub had no defects in MVB sorting, even in combination. This led us to search for additional UBDs within ESCRT-I and resulted in the discovery of a novel UBD within Mvb12. The UBD of Mvb12 works in concert with the UBDs of the ESCRTs to promote cargo recognition and MVB sorting.

Results and discussion

Mutants of Vps23 and Vps36 defective for Ub binding

Cocrystal structures of Ub with the UEV domains of Vps23 and TSG101 were used to guide mutagenesis experiments rendering Vps23 unable to bind Ub (Sundquist et al., 2004; Teo et al. 2004). The structures show that the UEV domains bind to Ub via a β hairpin tongue and a lip (Fig. 1 A). The structure of the

S.B. Shields and A.J. Oestreich contributed equally to this paper.

Correspondence to David J. Katzmann: katzmann.david@mayo.edu; or Robert Piper: Robert-piper@uiowa.edu

Abbreviations used in this paper: CPY, carboxypeptidase Y; ESCRT, endosomal sorting complexes required for transport; DIC, differential interference contrast; HSQC, heteronuclear single quantum coherence; MVB, multivesicular body; NMR, nuclear magnetic resonance; NZF, Npl4 zinc finger; TAP, tandem affinity purification; Ub, ubiquitin; UBD, Ub-binding domain; UEV, Ub E2 variant; UIM, Ub-interacting motif.

The Rockefeller University Press $30.00
J. Cell Biol. Vol. 185 No. 2 213–224
www.jcb.org/cgi/doi/10.1083/jcb.200811130

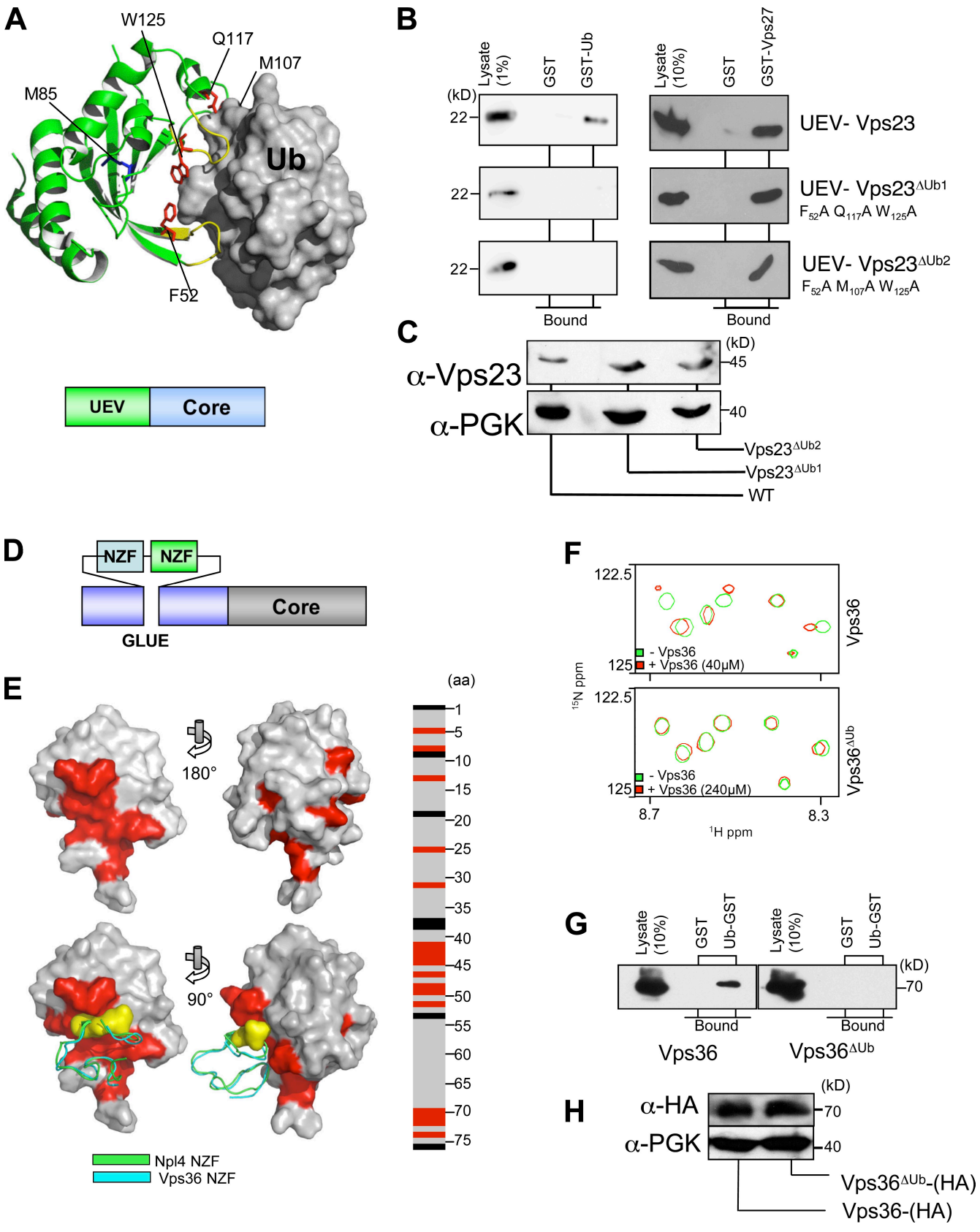

Figure 1. **Generation of Vps23 and Vps36 mutants incapable of binding Ub.** (A) Model of the Vps23 UEV domain in complex with Ub (Protein Data Bank accession no. 1UZX). The residues mutated to create the *vps23*$^{\Delta Ub}$ alleles are shown in red. (bottom) A schematic of the position of the UEV domain and the core region of Vps23 involved in complex formation with other ESCRT-I subunits is shown. (B) Recombinant V5 epitope–tagged wild-type and mutant Vps23 UEV domains were used for binding experiments with GST, Ub-GST, or GST-Vps27 C terminus. Bound proteins were immunoblotted with 1 or 10% of the input lysates. (C) Cell lysates from strains (PLY335, PLY3529, and PLY3530) bearing the wild-type (WT) or mutant alleles of *VPS23* were immunoblotted with

tongue interface is highly conserved and includes residues F_{52}-G_{57} of Vps23 and Y_{42}-G_{47} of TSG101. The lip of Vps23 contacts Ub with residues Q_{117} and W_{125}, which is different from TSG101 (Pornillos et al., 2002a,b). Two triple-mutant alleles of *VPS23* were generated: *vps23*$^{\Delta Ub1}$ (F_{52}A, Q_{117}A, and W_{125}A) and *vps23*$^{\Delta Ub2}$ (F_{52}A, M_{107}A, and W_{125}A). The corresponding UEV domains were expressed as V5 epitope–tagged proteins in bacteria and used for binding assays with GST-Ub. The wild-type UEV domain of Vps23 bound Ub, whereas no binding was observed for the mutant UEV domains (Fig. 1 B). However, all UEV domains bound to the C terminus of Vps27, which contains two PSDP motifs (P_{448}SDP and P_{524}SDP) that directly interact with Vps23 (Bilodeau et al., 2003). TSG101 has a similar interaction with PTAP motifs of viral *gag* proteins and Hrs (Pornillos et al., 2002a,b). Although the structural basis of the TSG101–PTAP interaction is known, it is not known for the Vps23–UEV–PSDP interaction, and the PTAP-binding pocket of TSG101 is not conserved in Vps23. Regardless, this demonstrated that the Vps23 UEV mutants are specifically defective for Ub binding and did not compromise expression of corresponding full-length Vps23 in vivo (Fig. 1 C).

Mutagenesis of the ESCRT-II subunit Vps36 was also performed. The Ub-binding activity of EAP45 (mammalian Vps36) is found within the N-terminal GLUE domain (Alam et al., 2006; Hirano et al., 2006). However, the GLUE domain of yeast Vps36 lacks these key elements of Ub binding. Instead, the yeast Vps36 GLUE domain has an insertion of two NZF domains, the second of which (NZF2) binds to Ub (Fig. 1 D; Alam et al., 2004). Ub binding was abolished by mutating $T_{187}F_{188}$ within the Vps36 NZF2 domain and $T_{13}F_{14}$ in the Npl4 NZF domain (Alam et al., 2004). Fig. 1 E shows the nuclear magnetic resonance (NMR) structure of Npl4-NZF-Ub, a modeled structure of the Vps36-NZF-Ub, and the predicted position of Vps36 residues $T_{187}F_{188}$ (Wang et al., 2003). We altered Vps36 $T_{187}F_{188}$ to $G_{187}A_{188}$ to make the Vps36$^{\Delta Ub}$ mutant. Ub binding was assessed in the context of the entire GLUE domain rather than just isolated NZF domains to ensure that Ub-binding activity was abolished. Mutation of Vps36 NZF2 was sufficient to abolish Ub binding by the GLUE domain. GST fusions of wild-type and Vps36$^{\Delta Ub}$ GLUE domains were assayed for binding to ^{15}N-labeled Ub by NMR heteronuclear single quantum coherence (HSQC) experiments (Fig. 1, E and F). The wild-type Vps36 GLUE gave distinct chemical shift changes in Ub. In contrast, the Vps36$^{\Delta Ub}$ GLUE domain, at a sixfold higher concentration, showed no chemical shift changes in Ub. V5 epitope–tagged wild-type and ΔUb GLUE domains of Vps36 were also used in binding assays with Ub-GST (Fig. 1 G). The wild-type Vps36 GLUE domain bound to Ub, but the Vps36$^{\Delta Ub}$ GLUE domain did not. The *ΔUb* mutation was then placed into the context of full-length Vps36 to create *vps36*$^{\Delta Ub}$. The mutations in Vps36 did not appear to have a deleterious effect on expression level because HA epitope–tagged alleles of *VPS36* and *vps36*$^{\Delta Ub}$ expressed from the endogenous *VPS36* promoter showed similar levels (Fig. 1 H).

Effect of inactivation of Vps23 and Vps36 Ub binding

To assess the role of Ub binding by Vps23 and Vps36, yeast strains were constructed in which the mutant alleles were integrated in place of the endogenous genes. We found that the inability of Vps23 or Vps36 to bind Ub had no effect on the sorting of GFP-Cps1, a model MVB cargo (Odorizzi et al., 1998), into the vacuolar lumen (Fig. 2 A). No difference was observed between the *vps23*$^{\Delta Ub1}$ or *vps23*$^{\Delta Ub2}$ alleles (unpublished data). Analysis of additional mutant *vps23* alleles with mutations in other residues that line the Ub interface (S_{56}, G_{57}, F_{105}, and N_{123}) also did not display any sorting defects (Fig. S1). Likewise, a double mutant containing *vps23*$^{\Delta Ub1}$ and *vps36*$^{\Delta Ub}$ showed normal sorting of GFP-Cps1 (Fig. 2 B). These results were confirmed using *vps23Δ* and *vps36Δ*-null mutants transformed with wild-type and *ΔUb* alleles of *VPS23* and *VPS36* housed on low copy plasmids (unpublished data). Lastly, sorting of other MVB cargoes, including Ste3-GFP (Urbanowski and Piper, 2001), Fur4-GFP (Blondel et al., 2004), and Sna3-GFP (Reggiori and Pelham, 2001) was normal in the *vps23*$^{\Delta Ub1}$ and *vps36*$^{\Delta Ub}$ alleles (unpublished data).

These findings differ from previous studies that found severe sorting defects upon mutation of the ESCRT-I UEV domain and the ESCRT-II NZF domain (Katzmann et al., 2001; Alam et al., 2004). Prior analysis of the UEV domain centered on a single mutant (M_{85}T) identified by a loss of function mutagenesis screen. M_{85} faces the interior of Vps23 and not the Ub-binding interface (Fig. 1 A). Thus, mutation of this residue may indirectly impact the ability of the UEV domain to bind to Ub or other factors. The NZF mutation used in this study was also distinct from previously described mutations that displayed MVB sorting defects (Alam et al., 2004). In both cases, mutations used in this study may maintain the overall integrity of Vps23 and Vps36 (based on in vivo function), although specifically ablating Ub binding (based on in vitro assays). Additionally, our functional analysis was performed with untagged, integrated alleles of *VPS23* and *VPS36*. The ability of the *vps23*$^{\Delta Ub}$ *vps36*$^{\Delta Ub}$ double mutant to successfully sort cargo into the MVB interior indicated that there might be additional UBDs within the ESCRT machinery.

Mvb12 binds Ub

A potential candidate for a protein with a novel UBD was Mvb12, a recently identified subunit of ESCRT-I. Previous studies

α-Vps23 and α-PGK (3-phosphoglycerate kinase) antibodies. (D) Schematic of Vps36 showing the GLUE domain with an insertion of two NZF domains, the second of which binds Ub. The core region of Vps36 interacts with the rest of ESCRT-I. (E) Summary of HSQC NMR experiments with ^{15}N-labeled Ub (25 μM) with the GLUE domains from wild-type Vps36 GLUE domain (40 μM) or Vps36$^{\Delta Ub}$ (240 μM). Chemical shift differences were quantified and plotted on the Ub sequence (right) or mapped on the Ub surface (left). Red indicates $(0.2\delta N^2 + \delta H^2)^{1/2} \geq 0.03$. Black residues were not observed. The models below show the NMR structure of Ub with the Npl4 NZF domain and a predicted structure of the Vps36 NZF domain. Yellow residues are the position of $T_{187}F_{188}$. (F) Portion of the HSQC spectra of ^{15}N-labeled Ub in the presence (red) and absence (green) of GST fusions of Vps36 and Vp36$^{\Delta Ub}$. ppm, parts per million. (G) V5 epitope–tagged Vps36 GLUE domains of wild-type or ΔUb were assayed for Ub binding with Ub-GST. Bound proteins were immunoblotted with 10% of the input lysates. (H) Cell lysates from wild-type strains expressing HA epitope–tagged alleles of wild-type *VPS36* and *vps36*$^{\Delta Ub}$ from low copy plasmids were immunoblotted with anti-HA and α-PGK.

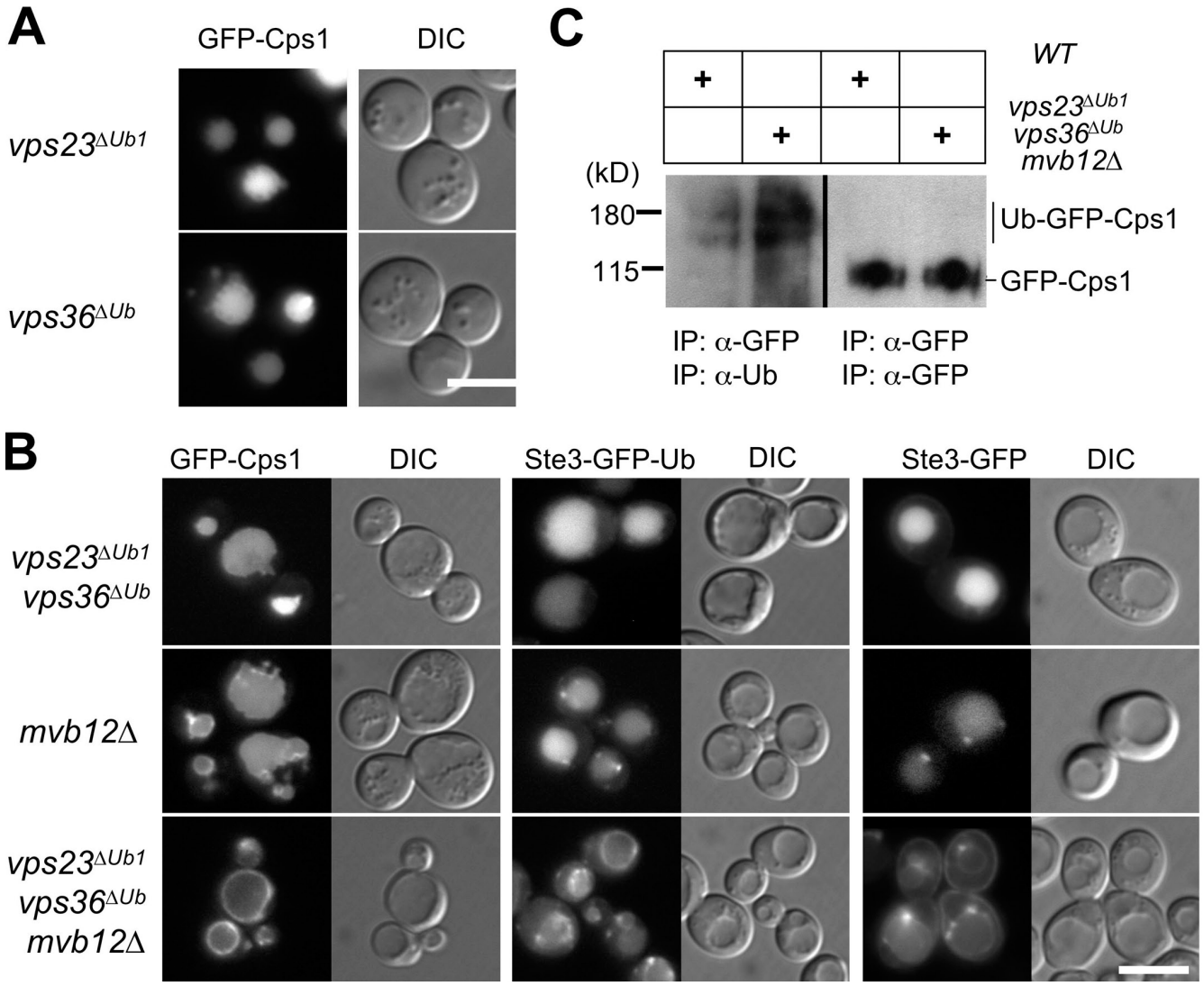

Figure 2. **Loss of Mvb12 reveals sorting defect of *vps23*$^{\Delta Ub}$ and *vps36*$^{\Delta Ub}$ mutants.** (A) GFP-Cps1 localization was assessed in *vps23*$^{\Delta Ub1}$ (PLY3528) and *vps36*$^{\Delta Ub}$ (PLY3395) cells. GFP fluorescence images along with matching DIC images are shown. (B) Sorting of GFP-Cps1, Ste3-GFP–Ub, and Ste3-GFP in *vps23*$^{\Delta Ub1}$ *vps36*$^{\Delta Ub}$ (PLY3522), *mvb12Δ*-null (JPY21), *vps23*$^{\Delta Ub1}$ *vps36*$^{\Delta Ub}$ *mvb12Δ* (PLY3623), and *vps23*$^{\Delta Ub1}$ *mvb12Δ* (PLY3624) cells. (C) GFP-Cps1 from wild-type (WT) and *vps23*$^{\Delta Ub1}$ *vps36*$^{\Delta Ub}$ *mvb12Δ* cells was immunoprecipitated with anti-GFP antibodies and immunoblotted with anti-Ub and anti-GFP antibodies. Black line indicates that intervening lanes have been spliced out. IP, immunoprecipitation. Bars, 5 µm.

showed that deletion of *MVB12* caused differential defects in MVB sorting; Ste3-GFP and Sna3-GFP display sorting defects, whereas GFP-Cps1, Ste2-GFP, and Ste3-GFP–Ub (in which Ub is fused in frame to the C terminus) sorting is largely unaffected (Chu et al., 2006; Curtiss et al., 2007; Oestreich et al., 2007). This indicates that Mvb12 plays a specific role in recognizing a subset of MVB cargoes. A role for Mvb12 cargo recognition was tested with strains that combined *vps23*$^{\Delta Ub1}$, *vps36*$^{\Delta ub}$, and *mvb12Δ* to probe for synthetic defects in MVB sorting. Combining these mutations caused dramatic sorting defects in GFP-Cps1 and Ste3-GFP (Fig. 2 B). The defect in sorting of GFP-Cps1 is not the result of a detectable loss of Cps1 ubiquitination (Fig. 2 C) but rather indicates a defect in recognition of Ub cargos. This was supported by examining the sorting of Ste3-GFP–Ub, which was normal in *mvb12Δ*-null and *vps23*$^{\Delta Ub1}$ *vps36*$^{\Delta Ub}$ double-mutant cells but defective in *vps23*$^{\Delta Ub1}$ *vps36*$^{\Delta Ub}$ *mvb12Δ* triple-mutant cells (Fig. 2 B).

The genetic interactions between Mvb12 and ESCRT-I and -II UBDs prompted us to determine whether Mvb12 could bind Ub. Recombinant V5 epitope–tagged full-length Mvb12 from *Saccharomyces cerevisiae* and the related budding yeast *Saccharomyces kluyveri* were used in binding assays with Ub-GST. Both proteins bound specifically to Ub-GST (Fig. 3 A). Deletion analysis of Mvb12 mapped the Ub binding to the C terminus (W_{50}-S_{101}; unpublished data). This interaction was confirmed by NMR HSQC experiments of ^{15}N-labeled Ub combined with the C terminus of Mvb12. Mvb12 induced chemical shift perturbations in the spectrum of ^{15}N-labeled Ub that mapped to a surface of Ub that included residues R_{42}, V_{70}, and L_8 (Fig. 3 E). This overlaps with the surface engaged by the Vps23 UEV domain, the Vps36 NZF domain, and the UIM domains of Vps27 and Hse1, indicating that simultaneous binding of these components to a single Ub molecule is unlikely (Bilodeau et al., 2003; Alam et al., 2004; Teo et al., 2004).

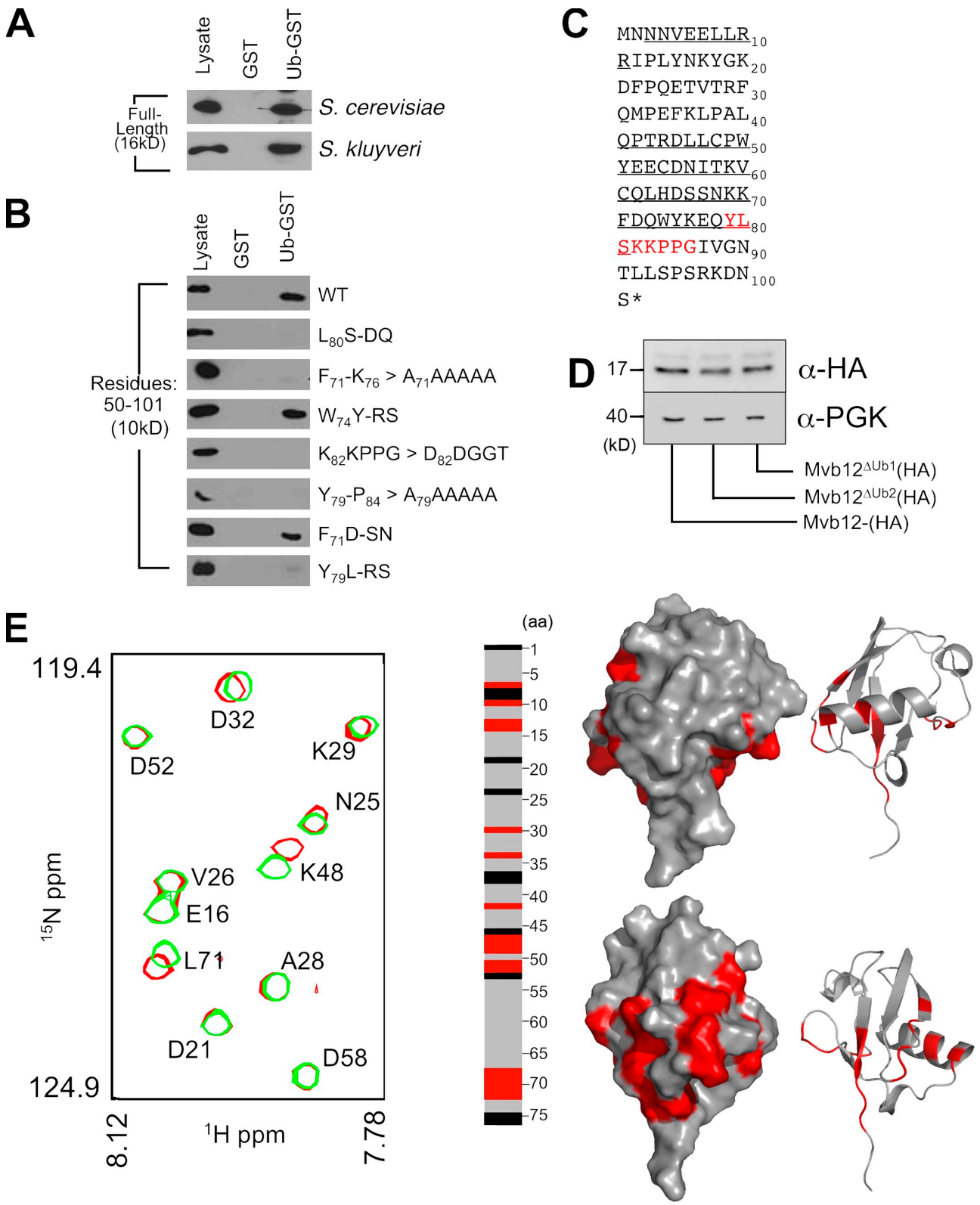

Figure 3. **Binding of Mvb12 to Ub.** (A) Recombinant V5 epitope–tagged Mvb12 for *S. cerevisiae* and *S. kluyveri* were assayed for Ub binding with Ub-GST. (B) V5 epitope–tagged fusions of the C terminus of either wild-type (WT) Mvb12 or the indicated mutants were expressed in bacteria and assayed for Ub binding with Ub-GST. (C) A sequence of Mvb12 with the Ub-binding region shown in red. Regions that make contact with Vps37 in the ESCRT-I crystal structure (Protein Data Bank accession no. 2P22) are underlined. The asterisk indicates the end of the protein sequence. (D) Cell lysates prepared from *mvb12Δ* cells transformed with low copy plasmids expressing Mvb12-HA (pPL3713), Mvb12$^{\Delta Ub1}$-HA (pPL3709), or Mvb12$^{\Delta Ub2}$-HA (pPL3711) were immunoblotted with anti-HA and anti-PGK antibodies. (E) Summary of NMR HSQC experiments with ^{15}N-labeled Ub (50 μM) with the C-terminal fragment of Mvb12 (100 μM). (left) Part of the spectra of ^{15}N-labeled Ub in the presence (red) and absence (green) of Mvb12 is shown. Chemical shift differences were quantified and plotted on the linear sequence of Ub (middle) or onto the surface of Ub (right). Red indicates $(0.2\delta N^2 + \delta H^2)^{1/2} \geq 0.02$. Black residues were not observed. ppm, parts per million.

The C-terminal fragment of Mvb12 was then mutated to produce a series of recombinant proteins that were subjected to Ub-GST–binding experiments. Mutations that disrupted Ub binding were localized to residues F_{71}-G_{84} as shown by two mutants with residues 71–76 and 79–84 replaced with alanines (Fig. 3 B). A recent crystal structure has shown that two patches of Mvb12, $F_{71}D_{72}$, and $W_{74}Y_{75}$ pack against a hydrophobic segment of Vps37 (Kostelansky et al., 2007). However, these residues did not seem critical for Ub binding, as mutation of $W_{74}Y$ to $R_{74}S$, and $F_{71}D$ to $S_{71}N$ did not block binding to Ub-GST (Fig. 3 B). In contrast, mutation of residues C terminal to this region abolished Ub binding. Interestingly, in the context of the entire ESCRT-I, the UBD of Mvb12 would be oriented near the UEV domain of Vps23, suggesting that both of these UBDs are close in native ESCRT-I.

Contribution of Mvb12 Ub binding to MVB sorting

We initially assessed the function of wild-type and the two Mvb12 Ub-binding mutants as HA epitope–tagged proteins expressed from low copy plasmids containing the native *MVB12* promoter. All three proteins expressed at comparable levels (Fig. 3 D), and all coprecipitated with Vps23 and Vps28, demonstrating that they properly assembled with ESCRT-I (Fig. 4 A). Gel filtration showed that tandem affinity purification (TAP)–tagged $Mvb12^{\Delta Ub1}$ (Y_{79}-G_{85}>A_{79}AAAAA) supported assembly into a large complex with an apparent molecular mass of 350 kD, as has been previously observed for ESCRT-I (Fig. S2). Furthermore, GFP-tagged $Mvb12^{\Delta Ub1}$ localized to endosomal compartments similar to GFP-tagged wild-type Mvb12 (Fig. S2). These data indicate that these Mvb12 mutants were able to assemble into the ESCRT-I complex. This allowed us to ascribe phenotypes to a deficiency in Ub binding of Mvb12 rather than loss of ESCRT-I association.

Cells expressing $mvb12^{\Delta Ub1}$ or $mvb12^{\Delta Ub2}$ (K_{82}KPPG> D_{82}DGGT) as their sole source of *MVB12* showed no sorting defects for Ste3-GFP or Sna3-GFP (Fig. 4 B). Agreeing with previous studies, Ste3-GFP and to large extent Sna3-GFP showed defective sorting in *mvb12Δ*-null cells (Fig. 4 C; Chu et al., 2006; Curtiss et al., 2007; Oestreich et al., 2007). Other MVB cargo proteins such as GFP-Cps1 and Ste3-GFP–Ub were normal (unpublished data). The same results were obtained with wild-type or chromosomally integrated $mvb12^{\Delta Ub}$ mutants (unpublished data).

Together, these data indicate that the mutations used to ablate Ub binding did not indiscriminately compromise Mvb12 function. They also implied that the function of Ub binding by Mvb12 alone is not critical for MVB sorting. We next assessed the role of the Mvb12 UBD in cells lacking the UBDs of Vps23 and Vps36 (Fig. 4 C). The $vps23^{\Delta Ub1}$ $vps36^{\Delta Ub}$ *mvb12Δ* triple mutant was cotransformed with low copy plasmids expressing wild-type *MVB12*, $mvb12^{\Delta Ub1}$, or $mvb12^{\Delta Ub2}$ and GFP-tagged MVB cargos. We found that wild-type *MVB12* conferred proper sorting of all cargos, whereas both $mvb12^{\Delta Ub}$ alleles showed defective sorting of GFP-Cps1 when combined with $vps23^{\Delta Ub}$ and $vps36^{\Delta Ub}$. These data show that the UBDs of Mvb12, Vps23, and Vps36 work jointly to efficiently sort MVB cargo because sorting was defective only when mutations were combined (Fig. 2 B and Fig. 4 C).

In contrast to the sorting of GFP-Cps1, other MVB cargos were sorted normally in the $vps23^{\Delta Ub}$ $vps36^{\Delta Ub}$ $mvb12^{\Delta Ub}$ triple mutants. These cargos included Sna3-GFP and Ste3-GFP (Fig. 4 C). This demonstrated that some degree of Ub-dependent MVB sorting was still intact and that there might be other ESCRT components that contribute to MVB cargo recognition; one candidate is Vps27–Hse1 (ESCRT-0). The Vps27–Hse1 complex contains three UIMs and binds the Vps23 UEV domain via its two PSDP motifs within the C terminus (P_{448}SDP and P_{524}SDP). Although deletion of *VPS27* altogether blocks ESCRT-I localization to endosomes (Katzmann et al., 2003), little phenotype is observed when the protein–protein interface between ESCRT-0 and ESCRT-I is disrupted by mutation of the two PSDP motifs in Vps27 ($Vps27^{\Delta Vps23}$, AA_{448}ADP and P_{524}AAA; Bilodeau et al., 2003). Localization of Vps23-GFP to endosomes was unperturbed as was recruitment of mCherry-tagged ESCRT-III subunit Vps20 (Fig. S1). To investigate whether the interaction with ESCRT-0 helped maintain sorting of MVB cargos in the $vps23^{\Delta Ub1}$ $vps36^{\Delta Ub}$ $mvb12^{\Delta Ub}$ strain, these mutations were combined with the $vps27^{\Delta Vps23}$ mutation. The resulting quadruple mutant displayed very significant sorting defects (Fig. 5 A). Sorting of all MVB cargoes was defective in $vps23^{\Delta Ub1}$ $vps36^{\Delta Ub}$ $vps27^{\Delta Vps23}$ $mvb12^{\Delta Ub}$ mutant cells. This included Ste-GFP, Ste3-GFP–Ub, and Sna3-GFP, which otherwise sorted normally in $vps23^{\Delta Ub1}$ $vps36^{\Delta Ub}$ $mvb12^{\Delta Ub}$ mutant cells (Fig. 4 C) or $vps23^{\Delta Ub}$ $vps36^{\Delta Ub}$ $vps27^{\Delta Vps23}$ cells (Fig. 5 A). These experiments clearly showed a critical contribution of the Mvb12 UBD because dramatic sorting defects were observed when the $mvb12^{\Delta Ub}$ $vps23^{\Delta Ub}$ $vps36^{\Delta Ub}$ and $vps27^{\Delta Vps23}$ alleles were combined. In spite of missorting MVB cargoes, the quadruple mutant cells were still capable of a residual level of sorting lipids into the interior lumenal membranes, indicated by sorting of the fluorescent lipid marker NBD-PC into the vacuole lumen. Unlike ESCRT-null mutants in which NBP-PC accumulates exclusively in endosomes (Bilodeau et al., 2002), NDB-PC accumulated within the vacuoles of $vps23^{\Delta Ub}$ $vps36^{\Delta Ub}$ $vps27^{\Delta Vps23}$ $mvb12^{\Delta Ub}$ cells (Fig. 5 B). Disruption of the Vps27–Vps23 interaction combined with mutation of the UBDs within ESCRT-I and -II revealed a separation of cargo sorting and MVB biogenesis.

Model for Ub-sorting receptors at the endosome

Our data show that Ub binding by Mvb12 is functionally important and contributes to the overall process of protein sorting into MVBs. Moreover, models proposed previously that require ubiquitinated cargo to be sequentially recognized by the UIMs of ESCRT-0, the Vps23 UEV domain of ESCRT-I, and the Vps36 component of ESCRT-II need to be amended. The available data support several functional models (Fig. 5 C) that can account for the multiple UBDs with the ESCRT network (Fig. 5 D). The one we favor is that ESCRTs function together as a large supercomplex that contains multiple UBDs, each of which can recognize and sort partially overlapping sets of ubiquitinated cargo. Multiple UBDs within this complex would enable recognition of Ub attached to a wide variety of membrane proteins or allow for

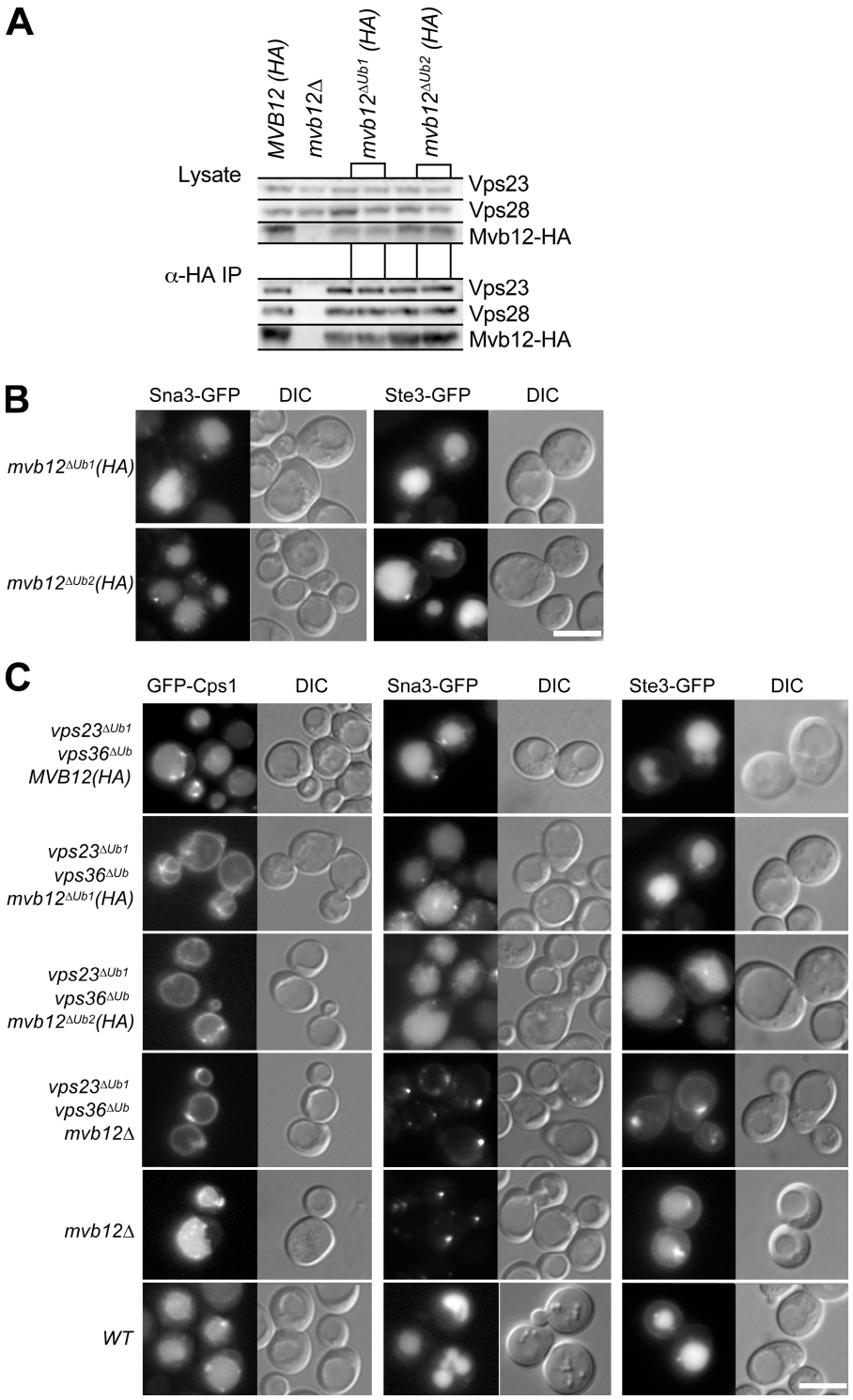

Figure 4. **Ub binding by Mvb12 contributes to GFP-Cps1 sorting.** (A) Mvb12 mutants lacking Ub binding correctly assemble with ESCRT-I. HA epitope–tagged wild-type Mvb12 and two mutants, *mvb12*$^{\Delta Ub1}$ and *mvb12*$^{\Delta Ub2}$, were expressed in *mvb12Δ* cells (pPL23713, pPL3709, and pPL3711 in JPY21). Lysates were prepared and immunoprecipitated with anti-HA antibodies and immunoblotted with α-Vps23, α-Vps28, or α-HA antibodies. IP, immunoprecipitation. (B) Sorting of Sna3-GFP and Ste3-GFP in *mvb12Δ* cells cotransformed with plasmids containing HA-tagged *mvb12ΔUb* alleles under the endogenous promoter. (C) Strains carrying the *mvb12*$^{\Delta Ub}$ alleles alone or in combination with *vps23*$^{\Delta Ub}$ and *vps36*$^{\Delta Ub}$ were assessed for MVB sorting using GFP-Cps1, Sna3-GFP, and Ste3-GFP. The *MVB12* alleles were expressed as HA epitope–tagged proteins from low copy plasmids (pPL23713, pPL3709, and pPL3711). Wild-type (WT), *mvb12Δ*-null, and *vps23*$^{\Delta Ub2}$ *vps36*$^{\Delta Ub}$ *mvb12Δ*–null cells were also analyzed. The GFP fluorescence images and corresponding DIC images are shown. Bars, 5 µm.

multiple cargo molecules per supercomplex. If this model were correct, then the observation that sorting of some cargo still occurs in the absence of Vps23, Vps36, and Mvb12 UBDs implies that there remain other UBDs within the ESCRT machinery. One possibility is that remaining UBDs are provided by components such as Vps27–Hse1 because disruption of the Vps27–Vps23 interface (the *vps27*$^{\Delta Vps23}$ mutation) caused a dramatic synthetic phenotype when combined with UBD mutations in Vps23, Vps36, and Mvb12. Alternatively, the UBDs of ESCRT-I and -II may perform other functions besides cargo recognition. In particular, coupled monoubiquitination of the ESCRT machinery itself, which has been observed in animal cells but not yet yeast, could cause UBDs to mediate a series of intra- and intermolecular interactions that could regulate assembly or efficiency of MVB sorting (Haglund and Stenmark, 2006; Hoeller et al., 2006). Indeed, the loss of UBDs in combination with the synthetic mutations that led to profound MVB-sorting defects also caused defects in vacuolar protein sorting (e.g., carboxypeptidase Y

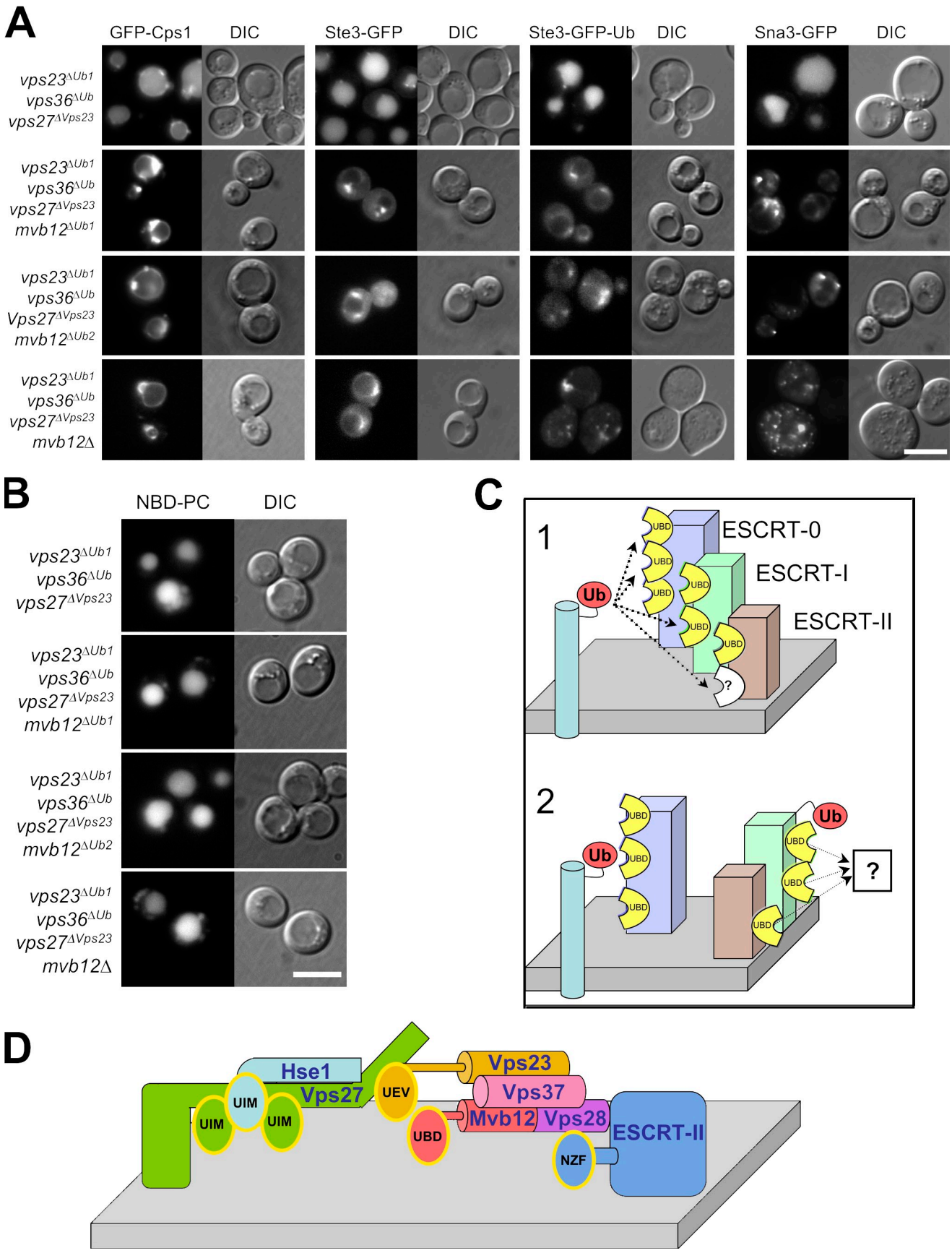

Figure 5. **Synthetic defects revealed by uncoupling ESCRT-0 from ESCRT-I.** (A) Strains (PLY3734, PLY3779, PLY3777, and PLY3781) of the indicated genotype were assessed for sorting of GFP-Cps1, Ste3-GFP, Ste3-GFP–Ub, and Sna3-GFP. All alleles were stably integrated into the genome as nonepitope

Table I. **Yeast strains used in this study**

Strain	Genotype	Source
SEY6210	*MATα leu2-3,112 ura3-52 his3-Δ200 trp1-Δ901 lys2-801 suc2-Δ9 mel*	Robinson et al., 1988
PLY3392	*vps36Δ::HIS3*	This study
PLY3394	*VPS36::TRP1::vps36Δ::HIS3*	This study
PLY3395	*vps36$^{\Delta Ub}$* ($T_{187}F/G_{188}A$)*::TRP1::vps36Δ::HIS3*	This study
PLY3405	*vps36$^{\Delta Ub}$::TRP1::vps36Δ::HIS3 vps23Δ::Kanr*	This study
PLY3407	*VPS36::TRP1::vps36Δ::HIS3 vps23Δ::Kanr*	This study
PLY3409	*vps36$^{\Delta Ub}$::TRP1::vps36Δ::HIS3 vps27Δ::Kanr*	This study
PLY3410	*VPS36::TRP1::vps36Δ::HIS3 vps27Δ::Kanr*	This study
PLY3522	*vps36$^{\Delta Ub}$::TRP1::vps36Δ::HIS3 vps23$^{\Delta Ub1}$* ($F_{52}A$ $Q_{117}A$ $W_{125}A$)	This study
PLY3528	*VPS36::TRP1::vps36Δ::HIS3 vps23$^{\Delta Ub1}$* ($F_{52}A$ $Q_{117}A$ $W_{125}A$)	This study
PLY3623	*vps36$^{\Delta Ub}$::TRP1::vps36Δ::HIS3 vps23$^{\Delta Ub1}$* ($F_{52}A$ $Q_{117}A$ $W_{125}A$) *mvb12Δ::plox*	This study
PLY3624	*VPS36::TRP1::vps36Δ::HIS3 vps23$^{\Delta Ub1}$* ($F_{52}A$ $Q_{117}A$ $W_{125}A$) *mvb12Δ::plox*	This study
PLY3725	*vps36$^{\Delta Ub}$::TRP1::vps36Δ::HIS3 vps23$^{\Delta Ub2}$* ($F_{52}A$ $M_{107}A$ $W_{125}A$) *vps27Δ::LEU2*	This study
PLY3734	*vps36$^{\Delta Ub}$::TRP1::vps36Δ::HIS3 vps23$^{\Delta Ub1}$* ($F_{52}A$ $Q_{117}A$ $W_{125}A$) *vps27$^{\Delta Vps23}$*	This study
PLY3744	*vps36$^{\Delta Ub}$::TRP1::vps36Δ::HIS3 vps23$^{\Delta Ub2}$* ($F_{52}A$ $M_{107}A$ $W_{125}A$) *vps27$^{\Delta Vps23}$ mvb12Δ::Kanr*	This study
PLY3776	*vps36$^{\Delta Ub}$::TRP1::vps36Δ::HIS3 vps23$^{\Delta Ub2}$* ($F_{52}A$ $M_{107}A$ $W_{125}A$) *mvb12Δ::plox MVB12::URA3*	This study
PLY3773	*vps36$^{\Delta Ub}$::TRP1::vps36Δ::HIS3 vps23$^{\Delta Ub2}$* ($F_{52}A$ $M_{107}A$ $W_{125}A$) *mvb12Δ::plox mvb12$^{\Delta Ub1}$::URA3*	This study
PLY3771	*vps36$^{\Delta Ub}$::TRP1::vps36Δ::HIS3 vps23$^{\Delta Ub2}$* ($F_{52}A$ $M_{107}A$ $W_{125}A$) *mvb12Δ::plox mvb12$^{\Delta Ub2}$::URA3*	This study
PLY3781	*vps36$^{\Delta Ub}$::TRP1::vps36Δ::HIS3 vps23$^{\Delta Ub2}$* ($F_{52}A$ $M_{107}A$ $W_{125}A$) *vps27$^{\Delta Vps23}$ mvb12Δ::Kanr MVB12::URA3*	This study
PLY3779	*vps36-ΔUb::TRP1::vps36Δ::HIS3 vps23$^{\Delta Ub2}$* ($F_{52}A$ $M_{107}A$ $W_{125}A$) *vps27$^{\Delta Vps23}$ mvb12Δ::Kanr mvb12$^{\Delta Ub1}$::URA3*	This study
PLY3777	*vps36$^{\Delta Ub}$::TRP1::vps36Δ::HIS3 vps23$^{\Delta Ub2}$* ($F_{52}A$ $M_{107}A$ $W_{125}A$) *vps27$^{\Delta Vps23}$ mvb12Δ::Kanr mvb12$^{\Delta Ub2}$::URA3*	This study
JPY21	*mvb12Δ::HIS3*	Oestreich et al., 2007

[CPY] secretion; Fig. S2), suggesting that UBDs may contribute to the general functions of the ESCRTs in a way that remains to be determined.

Materials and methods

Materials, yeast strains, and plasmids

Chemicals, antibodies, and, growth methods were used as previously described (Bilodeau et al., 2003; Ren et al., 2007). *S. cerevisiae* strains used in this study are listed in Table I. Plasmids used in this study are listed in Table II. *VPS36* was disrupted by inserting the *HIS3* gene in place of codons 101–539 of *VPS36*. Wild-type or *vps36$^{\Delta Ub}$* ($T_{187}F/G_{188}A$) cloned into the integrating *TRP1* plasmid pRS304 (pPL2646 and pPL2645, respectively) was linearized with ClaI and integrated at the *vps36Δ::HIS3* locus to make PLY3394 and PLY3395. The *vps23Δ::Kanr*, *mvb12Δ::Kanr*, and *vps27Δ::Kanr* disruptions were made by amplifying the respective loci from the BY4742 deletion collection (Winzeler et al., 1999) and transforming the PCR product into the appropriate strain. Vps27$^{\Delta Vps23}$ was made by integrating linearized integration plasmid pLP2251 digested with BlgII into the *URA3* loci of strains containing the *vps27Δ::LEU2* disruption. The *vps23$^{\Delta Ub}$* alleles were made by linearizing integrating pPL2940 into the *VPS23* loci of PLY3405 and PLY3407 and looping out the insertion of the *URA3* gene by selection of 5-FOA.

Unmarked disruption of *MVB12* was performed by replacing the *MVB12* ORF with *LEU2* and looping out with Cre recombinase as previously described (Gueldener et al., 2002).The *vps27Δ::LEU2* disruption was made by replacing codons 177–622 with *LEU2*. *MVB12* or *mvb12* alleles were at the *URA3* locus by transforming yeast with pPL3780, pPL3781, or pPL3784 linearized with StuI. HA-tagged Vps36 was made by integrating a triple HA epitope at the Vps36 C terminus made by homologous recombination with HA-containing host plasmid. Vps20-mCherry was made by amplifying the Vps20 ORF and 500 bp of the promoter from the genome and homologous recombining it with an mCherry-containing host plasmid.

HA epitope–tagged alleles of *MVB12* were made by inserting a single HA tag at the C terminus of *MVB12* followed by the *PHO8* 3′ untranslated region. Expression was driven by the *MVB12* promoter (500 bp region upstream of the *MVB12* ORF). Untagged *MVB12* alleles were made similarly but lacked the C-terminal tag. TAP- and GFP-tagged MVB12 alleles were made as previously described (Oestreich et al., 2007).

Glutathione agarose affinity chromatography

GST-fusion proteins were isolated from bacteria using glutathione-Sepharose beads as previously described (Smith and Johnson, 1988). For pull-down assays, 250 µg of each isolated GST fusion protein was bound to 50 µl glutathione-Sepharose in PBS by rotation for 30 min at 25°C. Bound GST or GST fusion proteins were pelleted and washed three times with PBS. Cell lysate was added to each protein/bead complex and incubated for 2 h at room temperature. Unbound proteins were removed from beads using three washes of cold PBS eluted with 50 µl 50 mM glutathione in PBS, pH 7.2, and the bound bead fraction was analyzed by SDS-PAGE and immunoblotting.

Fluorescence microscopy

Cells containing GFP-expressing plasmids were grown in synthetic dextrose minimal media to mid-log phase, resuspended in 0.2% NaN3 and 100 mM Tris, pH 8.0, and viewed using a 100× 1.4 NA aperture on a microscope (BX-60; Olympus) equipped with fluorescein isothiocyanate filters and Nomarski/differential interference contrast (DIC) optics at ambient temperature. Images were captured with a charge-coupled device camera

alleles under the control of their endogenous promoter. The GFP fluorescence images and corresponding DIC images are shown. (B) The same strains as in A were analyzed for sorting of the lipid marker NBD-PC. (C) Model for function of UBDs in the ESCRT machinery. Model 1 depicts the UBDs of ESCRT-0, -I, and -II acting together to present multiple binding sites for cargo. This model predicts that other UBDs are present in the ESCRT complexes. Model 2 shows that although UBDs of ESCRT-0 bind Ub cargo, the UBDs of ESCRT-I and -II may interact with Ub in other proteins and may regulate the assembly or activity of the MVB sorting apparatus. (D) Schematic of the various UBDs within the ESCRTs and the connections that tie the ESCRTs together in a supercomplex. Bars, 5 µm.

Table II. **Plasmids used in this study**

Plasmid	Description	Source
pPL2612	*vps36*$^{\Delta Ub}$ (T_{187}F G_{187}A)	This study
pPL2613	VPS36 (−309–1,698 VPS36 and 840 bp of the PHO8 3′UT) in pRS316	This study
pPL2612	*vps36*$^{\Delta Ub}$ (T_{187}F/G_{187}A) in pRS316	This study
pPL2645	*vps36*$^{\Delta Ub}$ (T_{187}F/G_{187}A) as a NotI–Acc65I fragment from pPL2612 in pRS304	This study
pPL2646	*VPS36* as a NotI–Acc65I fragment from pPL2613 in pRS304	This study
pPL2940	*vps23*$^{\Delta Ub1}$ in pRS306 ($F_{52}AQ_{117}AW125A$)	This study
pPL2180	*VPS23* (−598–1,298) as an XbaI–SacI fragment in pRS316 with BamHI site removed from polylinker with an XbaI–XhoI fill-in ligation	This study
pPL2447	*vps23* with UEV mutation F_{52}A in pPL2180	This study
pPL2448	*vps23* with UEV mutation N_{123}A in pPL2180	This study
pPL2449	*vps23* with UEV mutation W_{125}A in pPL2180	This study
pPL2451	*vps23* with UEV mutation $S_{55}AD_{56}$A in pPL2180	This study
pPL2452	*vps23* with UEV mutation $F_{52}AS_{55}AD_{56}$A in pPL2180	This study
pPL2453	*vps23* with UEV mutation $S_{55}AD_{56}AN_{123}$A in pPL2180	This study
pPL2465	*vps23* with UEV mutation S_{55}A in pPL2180	This study
pPL2466	*vps23* with UEV mutation S55AF_{105}A in pPL2180	This study
pPL2567	*vps23* with UEV mutation $F_{105}AW_{125}$A in pPL2180	This study
pPL2568	*vps23* with UEV mutation $F_{52}AF_{105}$A in pPL2180	This study
pPL2569	*vps23* with UEV mutation F_{105}A in pPL2180	This study
pPL2570	*vps23* with UEV mutation G_{57}A in pPL2180	This study
pPL2571	*vps23* with UEV mutation $G_{57}AF_{105}$A in pPL2180	This study
pPL2578	*vps23* with UEV mutation $F_{52}AW_{125}$A in pPL2180	This study
pPL2651	*vps23* with UEV mutation $F_{52}AN_{123}AW_{125}$A in pPL2180	This study
pPL2652	*vps23*$^{\Delta Ub1}$, UEV mutation $F_{52}AQ_{117}AW_{125}$A in pPL2180	This study
pPL2653	*vps23*$^{\Delta Ub2}$, UEV mutation $F_{52}AM_{107}AW_{125}$A in pPL2180	This study
pPL2654	*vps23* with UEV mutation $F_{52}AL_{102}AW_{125}$A in pPL2180	This study
pPL2655	*vps23* with UEV mutation Q_{117}A in pPL2180	This study
pPL2940	*vps23*$^{\Delta Ub1}$ from pPL2652 in pRS306	This study
pPL2941	*vps23*$^{\Delta Ub2}$ from pPL2653 in pRS306	This study
pPL3355	GST-Vps36 GLUE domain (residues 1–289)	This study
pPL3358	GST-Vps36$^{\Delta Ub}$ GLUE domain (residues 1–289)	This study
pPL3353	*VPS36* GLUE domain (residues 1–289) in pET151	This study
pPL3356	*vps36*$^{\Delta Ub}$ (residues 1–289) in pET151	This study
pPL2251	*vps27*$^{\Delta Vps23}$ in pRS306 PSD1 and PSD2 motifs mutated (AA_{448}ADP and P_{524}AAA)	This study
pPL3230	*MVB12* (aa 1–101) in pET151	This study
pPL3203	*MVB12* from *S. kluyveri* (aa 1–102) in pET151	This study
pPL3284	*MVB12* residues 56–101 in pET151	This study
pPL3543	*MVB12* residues 56–101 F_{71}DQWYK-A_{71}AAAA in pET151	This study
pPL3542	*MVB12* residues 56–101 L_{92}L-D_{92}Q in pET151	This study
pPL3544	*MVB12* residues 56–101 W_{74}Y-R_{74}S in pET151	This study
pPL3545	*MVB12* residues 56–101 K_{82}KPPG-D_{82}DGGT in pET151	This study
pPL3551	*MVB12* residues 56–101 Y_{79}LSKKPP-A_{79}AAAA in pET151	This study
pPL3552	*MVB12* residues 56–101 F_{71}D-S_{71}N in pET151	This study
pPL3709	*mvb12*$^{\Delta Ub1}$ Y_{79}LSKKPP-A_{79}AAAA with single HA tag in pRS316	This study
pPL3711	*mvb12*$^{\Delta Ub2}$ K_{82}KPPG-D_{82}DGGT with single HA tag in pRS316	This study
pPL3713	*MVB12* with single HA tag in pRS316	This study
pPL3780	*mvb12*$^{\Delta Ub2}$ K_{82}KPPG-D_{82}DGGT in pRS306	This study
pPL3781	*mvb12*$^{\Delta Ub1}$ Y_{79}LSKKPP-A_{79}AAAA in pRS306	This study
pPL3784	*MVB12* in pRS306	This study
NA	*MVB12-TAP* (TAP-tagged MVB12 driven by PRC1 promoter)	Oestreich et al., 2007
pAO94	*mvb12*$^{\Delta Ub1}$ Y_{79}LSKKPP-A_{79}AAAA -TAP (TAP-tagged mvb12 mutant driven by PRC1 promoter)	This study
NA	*MVB12-GFP* (GFP-tagged MVB12 driven by PRC1 promoter)	Oestreich et al., 2007
pAO104	*mvb12*$^{\Delta Ub1}$ Y_{79}LSKKPP-A_{79}AAAA -GFP (GFP-tagged mvb12 mutant driven by PRC1 promoter)	This study
NA	Ub-GST; expression plasmid for Ub fused to GST	Katzmann et al., 2001
pPL1945	GST-Vps27; expression plasmid for residues 353–610 of Vps27 fused to GST	Bilodeau et al., 2003
pGEX3x	GST expression plasmid	Smith and Johnson, 1988
NA	*VPS23*-GFP (GFP-tagged Vps23 driven by the endogenous promoter in pRS416)	Nickerson et al., 2006
pPL3982	Vps23$^{\Delta Ub1}$-GFP (GFP-tagged Vps23$^{\Delta Ub1}$ driven by endogenous promoter)	This study
pPL3979	*Vps20-mCherry* (mCherry-tagged Vps20 under the control of the endogenous promoter in pRS316)	This study

NA, not applicable.

(ORCA; Hamamatsu Photonics) with IPLABS software (BD) as previously described (Urbanowski and Piper, 1999). Image processing was performed in PhotoShop (CS; Adobe), where the original 12-bit images were converted to 8-bit images and the brightest pixel was set to 255. NBD-PC (1-myristoyl-2-[6-[(7-nitro-2-1,3-benzoxadiazol-4-yl)amino]hexanoyl]-sn-glycero-3-phosphocholine; Avanti Polar Lipids, Inc.) was used as previously described (Bilodeau et al., 2002).

NMR analysis

Recombinant proteins mixed with ^{15}N-labeled Ub were prepared as previously described (Bilodeau et al., 2004) or purchased from Spectra Stable Isotopes. [^{15}N]Ub HSQC spectra were collected on a 500-MHz spectrometer (Avance II US2; Bruker) and analyzed with SPARKY (T.D. Goddard and D.G. Kneller, SPARKY 3, University of California, San Francisco, San Francisco, CA) as previously described (Bilodeau et al., 2004). Chemical shift differences were calculated using the formula $(0.2\ \delta N^2 + \delta H^2)^{1/2}$. Binding experiments with Vps36 were performed in 50 mM $NaPO_4$, pH 7.2; binding experiments with Mvb12 were performed in 50 mM imidazole and 100 mM NaCl, pH 7.2. A spectrum of unbound ^{15}N-labeled Ub in the same buffer was used as the reference.

Other methods

Metabolic [^{35}S]methionine labeling and immunoprecipitation of CPY were performed as described previously (Cooper and Stevens, 1996). Preparation of yeast lysates for gel filtration, immunoblotting, and CPY pulse-chase analysis were performed as described previously (Oestreich et al., 2007). Protein models were drawn with the PyMOL molecular graphics system (http://pymol.sourceforge.net). A model for the Vps36 NZF domain was computed using the Wurst protein server (Torda et al., 2004).

Online supplemental materials

Fig. S1 shows the localization of GFP-Cps1 in strains with a range of mutations in Vps23, the structure of Vps23 UEV domain in complex with Ub highlighting mutated residues, the localization of Vps23-GFP, and Vps20-mCherry in strains containing *vps27*$^{\Delta vps23}$ mutations. Fig. S2 shows the localization of Mvb12-GFP, gel filtration experiments performed on wild-type and mutant Mvb12, and the results of CPY pulse-chase analysis of all of the strains used in this study. Online supplemental material is available at http://www.jcb.org/cgi/content/full/jcb.200811130/DC1.

Submitted: 24 November 2008
Accepted: 23 March 2009

References

Alam, S.L., J. Sun, M. Payne, B.D. Welch, B.K. Blake, D.R. Davis, H.H. Meyer, S.D. Emr, and W.I. Sundquist. 2004. Ubiquitin interactions of NZF zinc fingers. *EMBO J.* 23:1411–1421.

Alam, S.L., C. Langelier, F.G. Whitby, S. Koirala, H. Robinson, C.P. Hill, and W.I. Sundquist. 2006. Structural basis for ubiquitin recognition by the human ESCRT-II EAP45 GLUE domain. *Nat. Struct. Mol. Biol.* 13:1029–1030.

Bilodeau, P.S., J.L. Urbanowski, S.C. Winistorfer, and R.C. Piper. 2002. The Vps27p Hse1p complex binds ubiquitin and mediates endosomal protein sorting. *Nat. Cell Biol.* 4:534–539.

Bilodeau, P.S., S.C. Winistorfer, W.R. Kearney, A.D. Robertson, and R.C. Piper. 2003. Vps27-Hse1 and ESCRT-I complexes cooperate to increase efficiency of sorting ubiquitinated proteins at the endosome. *J. Cell Biol.* 163:237–243.

Bilodeau, P.S., S.C. Winistorfer, M.M. Allaman, K. Surendhran, W.R. Kearney, A.D. Robertson, and R.C. Piper. 2004. The GAT domains of clathrin-associated GGA proteins have two ubiquitin binding motifs. *J. Biol. Chem.* 279:54808–54816.

Blondel, M.O., J. Morvan, S. Dupre, D. Urban-Grimal, R. Haguenauer-Tsapis, and C. Volland. 2004. Direct sorting of the yeast uracil permease to the endosomal system is controlled by uracil binding and Rsp5p-dependent ubiquitylation. *Mol. Biol. Cell.* 15:883–895.

Chu, T., J. Sun, S. Saksena, and S.D. Emr. 2006. New component of ESCRT-I regulates endosomal sorting complex assembly. *J. Cell Biol.* 175:815–823.

Cooper, A.A., and T.H. Stevens. 1996. Vps10p cycles between the late-Golgi and prevacuolar compartments in its function as the sorting receptor for multiple yeast vacuolar hydrolases. *J. Cell Biol.* 133:529–541.

Curtiss, M., C. Jones, and M. Babst. 2007. Efficient cargo sorting by ESCRT-I and the subsequent release of ESCRT-I from multivesicular bodies requires the subunit Mvb12. *Mol. Biol. Cell.* 18:636–645.

Gruenberg, J., and H. Stenmark. 2004. The biogenesis of multivesicular endosomes. *Nat. Rev. Mol. Cell Biol.* 5:317–323.

Gueldener, U., J. Heinisch, G.J. Koehler, D. Voss, and J.H. Hegemann. 2002. A second set of loxP marker cassettes for Cre-mediated multiple gene knockouts in budding yeast. *Nucleic Acids Res.* 30:e23.

Haglund, K., and H. Stenmark. 2006. Working out coupled monoubiquitination. *Nat. Cell Biol.* 8:1218–1219.

Hirano, S., N. Suzuki, T. Slagsvold, M. Kawasaki, D. Trambaiolo, R. Kato, H. Stenmark, and S. Wakatsuki. 2006. Structural basis of ubiquitin recognition by mammalian Eap45 GLUE domain. *Nat. Struct. Mol. Biol.* 13:1031–1032.

Hoeller, D., N. Crosetto, B. Blagoev, C. Raiborg, R. Tikkanen, S. Wagner, K. Kowanetz, R. Breitling, M. Mann, H. Stenmark, and I. Dikic. 2006. Regulation of ubiquitin-binding proteins by monoubiquitination. *Nat. Cell Biol.* 8:163–169.

Hurley, J.H. 2008. ESCRT complexes and the biogenesis of multivesicular bodies. *Curr. Opin. Cell Biol.* 20:4–11.

Katzmann, D.J., M. Babst, and S.D. Emr. 2001. Ubiquitin-dependent sorting into the multivesicular body pathway requires the function of a conserved endosomal protein sorting complex, ESCRT-I. *Cell.* 106:145–155.

Katzmann, D.J., G. Odorizzi, and S.D. Emr. 2002. Receptor downregulation and multivesicular-body sorting. *Nat. Rev. Mol. Cell Biol.* 3:893–905.

Katzmann, D.J., C.J. Stefan, M. Babst, and S.D. Emr. 2003. Vps27 recruits ESCRT machinery to endosomes during MVB sorting. *J. Cell Biol.* 162:413–423.

Kostelansky, M.S., C. Schluter, Y.Y. Tam, S. Lee, R. Ghirlando, B. Beach, E. Conibear, and J.H. Hurley. 2007. Molecular architecture and functional model of the complete yeast ESCRT-I heterotetramer. *Cell.* 129:485–498.

Nickerson, D.P., M. West, and G. Odorizzi. 2006. Did2 coordinates Vps4-mediated dissociation of ESCRT-III from endosomes. *J. Cell Biol.* 175:715–720.

Odorizzi, G., M. Babst, and S.D. Emr. 1998. Fab1p PtdIns(3)P 5-kinase function essential for protein sorting in the multivesicular body. *Cell.* 95:847–858.

Oestreich, A.J., B.A. Davies, J.A. Payne, and D.J. Katzmann. 2007. Mvb12 is a novel member of ESCRT-I involved in cargo selection by the multivesicular body pathway. *Mol. Biol. Cell.* 18:646–657.

Piper, R.C., and D.J. Katzmann. 2007. Biogenesis and function of multivesicular bodies. *Annu. Rev. Cell Dev. Biol.* 23:519–547.

Pornillos, O., S.L. Alam, D.R. Davis, and W.I. Sundquist. 2002a. Structure of the Tsg101 UEV domain in complex with the PTAP motif of the HIV-1 p6 protein. *Nat. Struct. Biol.* 9:812–817.

Pornillos, O., S.L. Alam, R.L. Rich, D.G. Myszka, D.R. Davis, and W.I. Sundquist. 2002b. Structure and functional interactions of the Tsg101 UEV domain. *EMBO J.* 21:2397–2406.

Reggiori, F., and H.R. Pelham. 2001. Sorting of proteins into multivesicular bodies: ubiquitin-dependent and -independent targeting. *EMBO J.* 20:5176–5186.

Ren, J., Y. Kee, J.M. Huibregtse, and R.C. Piper. 2007. Hse1, a component of the yeast Hrs-STAM ubiquitin-sorting complex, associates with ubiquitin peptidases and a ligase to control sorting efficiency into multivesicular bodies. *Mol. Biol. Cell.* 18:324–335.

Robinson, J.S., D.J. Klionsky, L.M. Banta, and S.D. Emr. 1988. Protein sorting in *Saccharomyces cerevisiae*: isolation of mutants defective in the delivery and processing of multiple vacuolar hydrolases. *Mol. Cell. Biol.* 8:4936–4948.

Shih, S.C., D.J. Katzmann, J.D. Schnell, M. Sutanto, S.D. Emr, and L. Hicke. 2002. Epsins and Vps27p/Hrs contain ubiquitin-binding domains that function in receptor endocytosis. *Nat. Cell Biol.* 4:389–393.

Slagsvold, T., R. Aasland, S. Hirano, K.G. Bache, C. Raiborg, D. Trambaiolo, S. Wakatsuki, and H. Stenmark. 2005. Eap45 in mammalian ESCRT-II binds ubiquitin via a phosphoinositide-interacting GLUE domain. *J. Biol. Chem.* 280:19600–19606.

Smith, D.B., and K.S. Johnson. 1988. Single-step purification of polypeptides expressed in *Escherichia coli* as fusions with glutathione S-transferase. *Gene.* 67:31–40.

Sundquist, W.I., H.L. Schubert, B.N. Kelly, G.C. Hill, J.M. Holton, and C.P. Hill. 2004. Ubiquitin recognition by the human TSG101 protein. *Mol. Cell.* 13:783–789.

Teo, H., D.B. Veprintsev, and R.L. Williams. 2004. Structural insights into endosomal sorting complex required for transport (ESCRT-I) recognition of ubiquitinated proteins. *J. Biol. Chem.* 279:28689–28696.

Torda, A.E., J.B. Procter, and T. Huber. 2004. Wurst: a protein threading server with a structural scoring function, sequence profiles and optimized substitution matrices. *Nucleic Acids Res.* 32:W532–W535.

Urbanowski, J.L., and R.C. Piper. 1999. The iron transporter Fth1p forms a complex with the Fet5 iron oxidase and resides on the vacuolar membrane. *J. Biol. Chem.* 274:38061–38070.

Urbanowski, J.L., and R.C. Piper. 2001. Ubiquitin sorts proteins into the intralumenal degradative compartment of the late-endosome/vacuole. *Traffic.* 2:622–630.

Wang, B., S.L. Alam, H.H. Meyer, M. Payne, T.L. Stemmler, D.R. Davis, and W.I. Sundquist. 2003. Structure and ubiquitin interactions of the conserved zinc finger domain of Npl4. *J. Biol. Chem.* 278:20225–20234.

Winzeler, E.A., B. Lee, J.H. McCusker, and R.W. Davis. 1999. Whole genome genetic-typing in yeast using high-density oligonucleotide arrays. *Parasitology.* 118(Suppl):S73–S80.